Project 5: Diffraction and Fourier Optics

Gianfranco Grillo

November 13th, 2017

Abstract

We present and discuss the results of a series of basic optical experiments where we have studied the phenomena of diffraction and applied Fourier analysis to optical systems. We study the diffraction patterns of collimated HeNe laser light as it passes through different types of apertures and objects, and examine the deviations from ideal Fraunhofer diffraction patterns. We also measure the wavelength of the laser light by measuring the distances between maxima of the diffraction pattern due to a grating, attempt to reproduce the Talbot effect, and set up a coherent optical computer in order to demonstrate the Fourier transformation properties of lenses. We find good agreement between the observed and expected diffraction patterns for the objects and apertures studied. We measured the laser light's wavelength to be 641 ± 6 nm which is very close to the nominal value of 632.8 nm. We were unable to observe the Talbot effect, although we were able to see how the diffraction pattern of the mesh grid changed depending on the position of the image plane. The coherent optical computer worked as expected, and we found agreement between observations and the expected results based on numerical simulations.

1 Introduction

The wave nature of electromagnetic radiation gives rise to diffraction phenomena, whereupon the wavefronts bend and interfere among themselves as the radiation propagates through an aperture or obstacle. The ways in which these interference effects manifest themselves are extremely diverse, and often counterintuitive. Rigorous study of diffraction is in general associated with the utilization of complex mathematical techniques, and in practice there are only a few situations in which physical problems involving diffraction can be solved exactly, so the application of physically reasonable approximations and numerical methods are an essential part of the study of diffraction phenomena.

One of the most important mathematical techniques that can be applied to the resolution of diffraction problems is the Fourier transform, as many of the integrals that arise in the study of diffraction effects have the form of the protoypical Fourier integrals. The study of classical optics from the point of view of Fourier transforms, where the propagating waves are regarded as a superposition of plane waves, is known as Fourier optics. The advent of electronic computers and the development of the Fast Fourier Transform has resulted in Fourier optics becoming an essential tool in the resolution of optical problems involving diffraction.

In this project, we study some of diffractive effects in the near field (Fresnel) and far field (Fraunhofer) regimes, and show how certain optical elements, like lenses, can be regarded as physical manifestations of the Fourier transform.

We perform the data analysis using Python and the associated libraries NumPy and SciPy ([1]), as well as the Uncertainty package ([2]).

2 Theoretical background

2.1 Diffraction patterns in the Fraunhofer limit

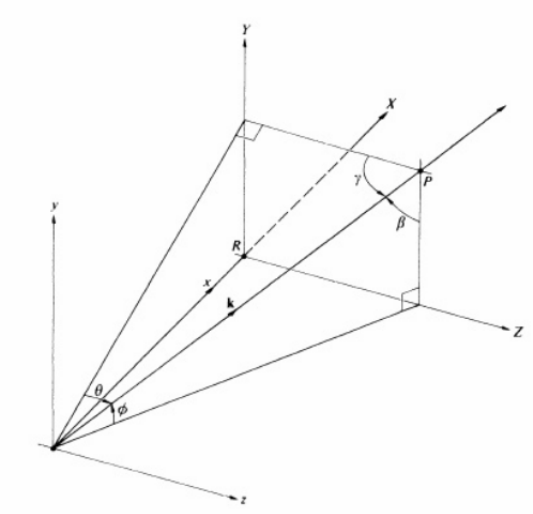

Figure 1: Diffraction geometry. Obtained from [3].

The analysis of diffractive effects can be separated into two regimes: Fresnel (or near field) diffraction and Fraunhofer (or far field) diffraction. In general, an electromagnetic wave that is radiated by a point source has a non-zero curvature that decreases in a manner directly proportional to the square of the propagated distance. Near field diffraction occurs when the diffractive object or aperture is close enough to the source, and the observer is close enough to the aperture, that the curvature of the incident wave cannot be neglected for the purposes of describing the resulting diffraction pattern. In the Fraunhofer limit, on the other hand, the distances between the source and the aperture and the aperture and the observer are sufficiently large such that it is possible to treat the waves incident on the aperture and the observer as plane waves. More quantitatively, if b is the size of the aperture or obstacle, λ is the wavelength of the radiation, and R is the smallest of either the source-aperture distance or the aperture-observer distance, then the Fraunhofer approximation applies when

$$R > \frac{b^2}{\lambda} \tag{1}$$

The first experiment of this project compares expected Fraunhofer diffraction patterns of different apertures and obtacles to ones obtained in the laboratory. We will not derive the pattern for each of the apertures; suffice is to say that they can be obtained by solving the Kirchoff diffraction integral in the Fraunhofer limit. This integral describes the electric field E at the observer's position (Y, Z), and is given by

$$E(Y,Z) = \iint_{-\infty}^{\infty} \mathcal{A}(y,z) \exp\left[\frac{\imath k(Yy + Zz)}{R}\right] dxdy \tag{2}$$

where y and z are the coordinates in a point at the aperture, and $\mathcal{A} = \mathcal{A}_0(y,z)e^{\imath\phi(y,z)}$ is known as the aperture function, which describes the amplitude of the field over the aperture. The function $\phi(y,z)$ describes the variation of the phase in the yz plane, and $k = \frac{2\pi}{\lambda}$ is the wavenumber. An illustration of the geometry can be found in Figure 1. The limits of the integral in (2) are from $-\infty$ to ∞, because the aperture function can be regarded to be zero everywhere except at the region that corresponds to the aperture. Evaluation of this integral for an appropriate choice of aperture function allows us to find the far field irradiance pattern of a particular kind of aperture. A more detailed analysis can be found in chapter 11 of [3], and chapters VIII and XI of [4].

Table 1 shows the expected irradiance of the diffraction patterns for each of the apertures used in experiment 1. By Babinet's principle, the far field diffraction patterns for an aperture is the same as the far field diffraction patterns for its complementary obstacle. This means irradiance pattern for the circular aperture with radius r is the same as the pattern for an opaque circular obstacle of radius r, and the irradiance pattern of a single slit of width a is the same as the pattern for a wire with the same width.

Type of aperture	Normalized irradiance I/I_0	Definitions
Single slit	$\operatorname{sinc}^2\left(\frac{a\pi x}{\lambda\sqrt{x^2+d^2}}\right)$	$a =$ slit width $d =$ slit-screen distance $x =$screen coordinates
Multiple slits	$\operatorname{sinc}^2\beta\left[\frac{\sin(N\alpha)}{N\sin\alpha}\right]^2$	$\beta = \frac{a\pi x}{\lambda\sqrt{x^2+d^2}}$ $\alpha = \frac{b\pi x}{\lambda\sqrt{x^2+d^2}}$ $b =$slit separation
Circular	$\left[\frac{2J_1(\gamma)}{\gamma}\right]^2$	$J_1(\gamma) = \frac{1}{2\pi\imath}\int_0^{2\pi} e^{\imath(v+\gamma\cos v)}\,dv$ $\gamma = \frac{2\pi r x}{\lambda\sqrt{x^2+d^2}}$ $r =$aperture radius

Table 1: Fraunhofer diffraction irradiance patterns for different apertures.

2.2 Diffraction grating maxima

Diffraction gratings are essentially a multiple slits aperture with large N and small separation $b > a$. The transmission diffraction grating, in fact, is just that. It is possible to determine the wavelength of the light that passes through a diffraction grating in a simple way, by measuring the distance between the positions of the maxima at a screen. Let s_m be the separation between the zeroth order maximum and the maxima of order m, and d be the distance from the diffraction grating to the screen, and the wavelength of the light will be given by

$$\lambda = \frac{bs_m}{m\sqrt{s_m^2 + m^2d^2}} \tag{3}$$

This is known as the grating formula. A complete derivation can be found in chapter 10 of [3]. We will make use of this equation in experiment 2 in order to calculate the wavelength of the laser light.

2.3 The Talbot effect

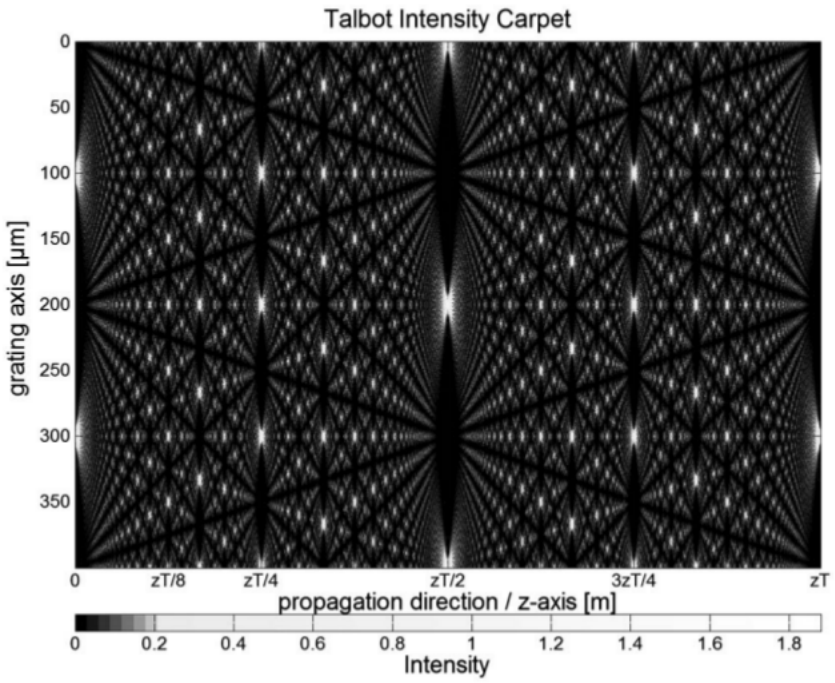

Figure 2: The Talbot carpet. Obtained from [6].

The Talbot effect is the name given to the fractal phenomenon that occurs when a two dimensional diffraction grating is illuminated by a source of coherent, monochromatic light. If a grating with period a is illuminated with monochromatic light of wavelength λ, and a movable screen is placed some distance away from the grating, a diffraction pattern will be observed on the screen. If the screen is now moved by a distance Δz, the characteristics of the diffraction pattern at the screen will change. However, after the screen has been moved a distance equal to the Talbot length z_T, the original pattern will become visible again. This characteristic length is given by

$$z_T = \frac{a^2}{\lambda} \tag{4}$$

Figure 2 shows an illustration of this effect, the so-called Talbot carpet. The mathematics underlying this phenomenon are not simple, and a more detailed analysis will not be pursued here. An in-depth overview of the effect can be found in [5]. In experiment 3, we will attempt to observe this effect using a laser and a rectangular wire mesh. In order to quantitatively compare the shapes of the obtained diffraction patterns, we will use the structural similarity index. For two images x and y represented as matrices of size NxN, the index is defined by

$$SSIM(x,y) = \frac{(2\mu_x\mu_y + c_1)(2\sigma_{xy} + c_2)}{(\mu_x^2 + \mu_y^2 + c_1)(\sigma_x^2 + \sigma_y^2 + c_2)} \tag{5}$$

where μ_x and μ_y are the average value of each of the matrices, σ_x^2 and σ_y^2 their respective variances, σ_{xy} their covariance, and c_1, c_2 two technical parameters used to stabilize the function when the averages and variances are small. The index is designed in such a way that it is always positive, identical images have an $SSIM = 1$, and the less similar the images are, the smaller the index becomes. A more detailed analysis of the concept and the reasoning behind it can be found in [7].

2.4 The lens as a Fourier transform and the coherent optical computer

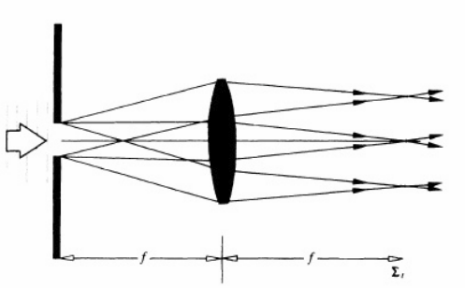

Figure 3: The lens as a Fourier transform. Obtained from [3].

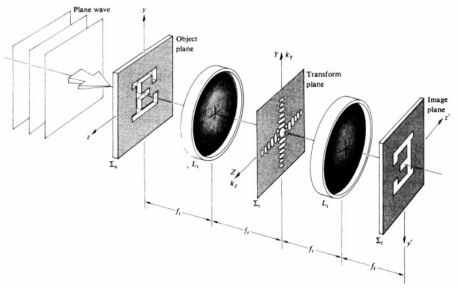

Figure 4: The coherent optical computer. Obtained from [3].

The Fourier transform of a function of two variables $f(x, y)$ is defined by the double integral

$$F(k_x, k_y) = \mathcal{F}\{f(x,y)\} = \iint_{-\infty}^{\infty} f(x,y) \exp\left[\imath(k_x x + k_y y)\right] \tag{6}$$

where k_x, k_y are the angular frequencies in each of the axes. A converging lens placed a distance equal to the focal length from a diffractive object that is being illuminated by collimated light will convert the near field diffraction pattern emerging from the object into a far field diffraction pattern that can be observed if one places a screen at the lens's back focal point (Figure 3). This diffraction pattern can be found by solving the integral in (2), which is nothing more than the Fourier transform of the aperture function. Define $\mathrm{k}_y = \frac{kY}{R}$, $\mathrm{k}_z = \frac{kZ}{R}$, and the integral can be written as

$$\begin{aligned} E(Y,Z) &= \iint_{-\infty}^{\infty} \mathcal{A}(y,z) \exp\left[\imath(\mathrm{k}_y y + \mathrm{k}_z z)\right] dydz \\ &= \mathcal{F}\{\mathcal{A}(y,z)\} \end{aligned} \tag{7}$$

In such a configuration, then, the lens acts as a Fourier transformer. Conceptually, the Fourier transform maps a function from its space or time domain into its spatial or angular frequency domain. This implies that it is possible to build an optical system that can filter certain spatial frequencies emerging from a diffraction pattern by placing a lens at a focal distance away from a diffractive object, and then placing a filter at the lens back focal point. If one also places another lens at a focal length away from the filter, this lens will act as an inverse Fourier transformer, and the filtered image can be seen at a screen placed a focal distance away from this second lens. This arrangement is shown

in Figure 4, and is known as the coherent optical computer. Mathematically, if the irradiance of the diffraction pattern at the screen without a filter is given by $f(y,z)$, then the irradiance I of the diffraction pattern that one obtains when using a filter with aperture function $\mathcal{A}(y,z)$ is given by

$$I = \mathcal{F}^{-1}\left[\mathcal{F}\left\{f(y,z)\right\} \cdot \mathcal{A}(y,z)\right] \tag{8}$$

where the dot corresponds to term by term multiplication when the functions are substantiated as matrices. What this means is that, given an image of the unfiltered pattern, it is possible to numerically recreate what the image should be when one places a filter at the transform plane by applying (8) using an appropriate choice of $\mathcal{A}(y,z)$. We will do this in the last experiment of this project. For a more detailed analysis of the coherent optical computer and Fourier optics in general, see chapters 11 and 13 of [3].

3 Experimental Set-Up and Results

3.1 Experiment 1

3.1.1 Set-Up

In this experiment, we measure the diffraction patterns for several different types and obstacles and compare them with the theoretical diffraction patterns in the Fraunhofer limit, which are given in Table 1. We set up a spatial filter using a 25 mm converging lens and a pinhole separated by a distance of 25 mm, and expand the beam using a 50 mm lens placed 50 mm away from the pinhole. We now set up a target assembly a distance R_1 away from the second lens, and a beam stopper a distance R_2 from the target assembly, such that the Fraunhofer criterion (1) is satisfied for all apertures used. We proceed to place a particular aperture at the target assembly and take a picture of its diffraction pattern at the beam stopper using a camera from a Samsung Galaxy S7. We repeat the procedure for different kinds of apertures.

3.1.2 Results and analysis

We used distances $R_1 = 38.3 \pm 0.3$ cm and $R_2 = 41.0 \pm 0.3$ cm. For equation (1) to be satisfied, we then need R_1 to be greater than $\frac{b^2}{\lambda}$, where b denotes the size of the aperture. The largest aperture had $b = 0.25$ mm, and $\lambda = 632.8$ nm, which gives $\frac{b^2}{\lambda} \approx 10$ cm, which is less than R_1, so we expect the Fraunhofer criterion to apply for all apertures used in the experiment.

Figures 5 and 6 show the (vertically averaged and normalized) intensities of the diffraction patterns for each of the apertures used, as well as colormaps of the diffraction patterns themselves. We used single slits with widths a of 0.02 mm, 0.04 mm, and 0.08 mm, multiple slits apertures with $a = 0.04$ mm and $b = 0.125$ mm and N of 2, 3, 4, and 5, circular apertures with radii r of 0.04 mm and 0.05 mm, and single wire obstacles with widths of 0.08, 0.125, and 0.25 mm. Since the pictures were not all taken from the exact same distance, and the beam stopper did not have a scale on it, we determine the x-axis scale by eye depending on how the measured pattern fits with the theoretical one. A more accurate way would be to do it by taking the Fourier transform of both patterns and adjusting the scale such that both transforms overlap, but this was not deemed necessary for the purposes of this project.

The measured irradiance have the shapes that we expect on theoretical grounds, like the figures show, except for the fact that the central region appears to be elevated, and faint spots are more visible in the experimental patterns than in the theoretical ones. The reason for this is that the brightness

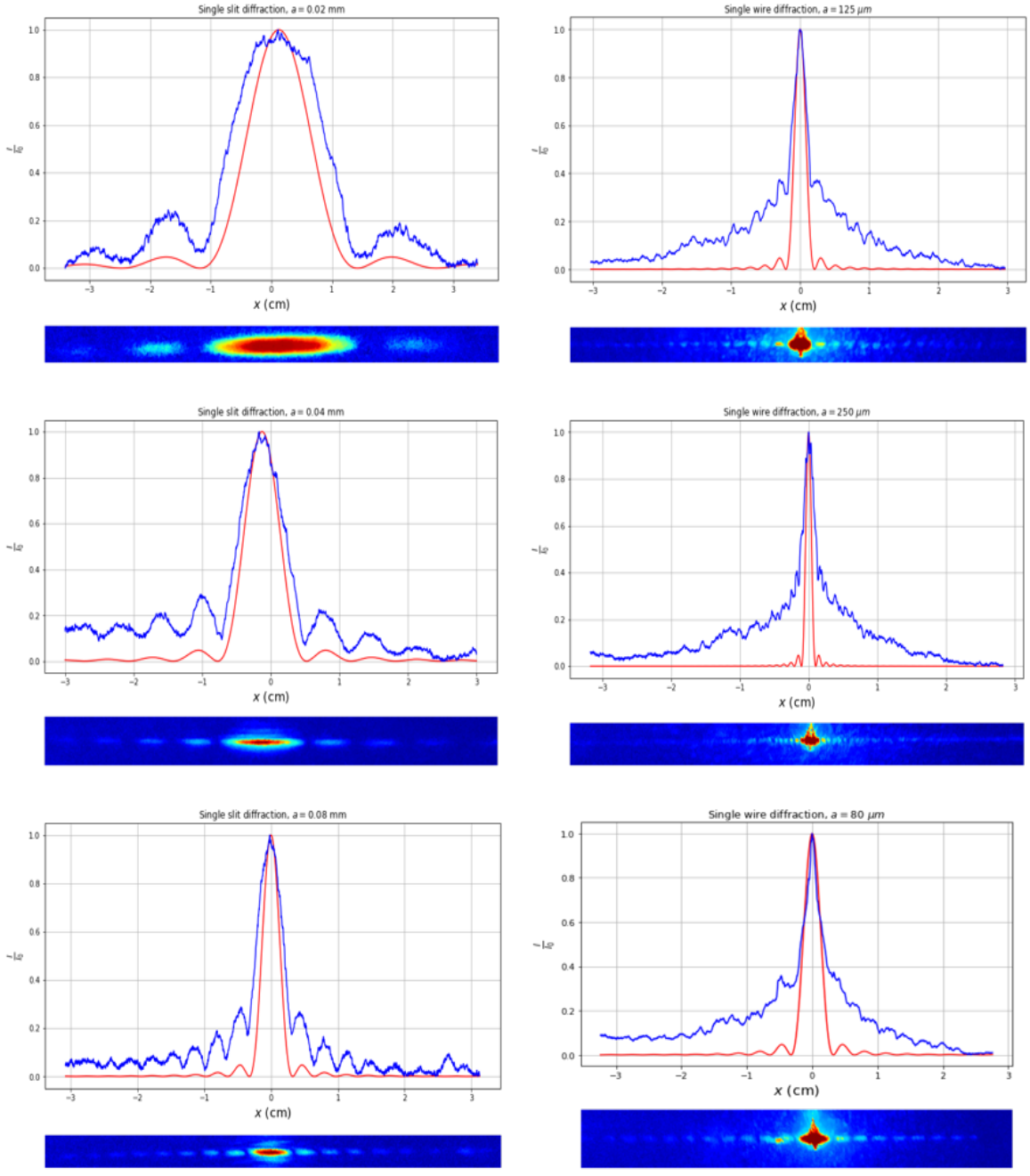

Figure 5: Diffraction patterns for single slits and wires. The blue curve is the measured normalized irradiance, and the red curve is the theoretical diffraction curve.

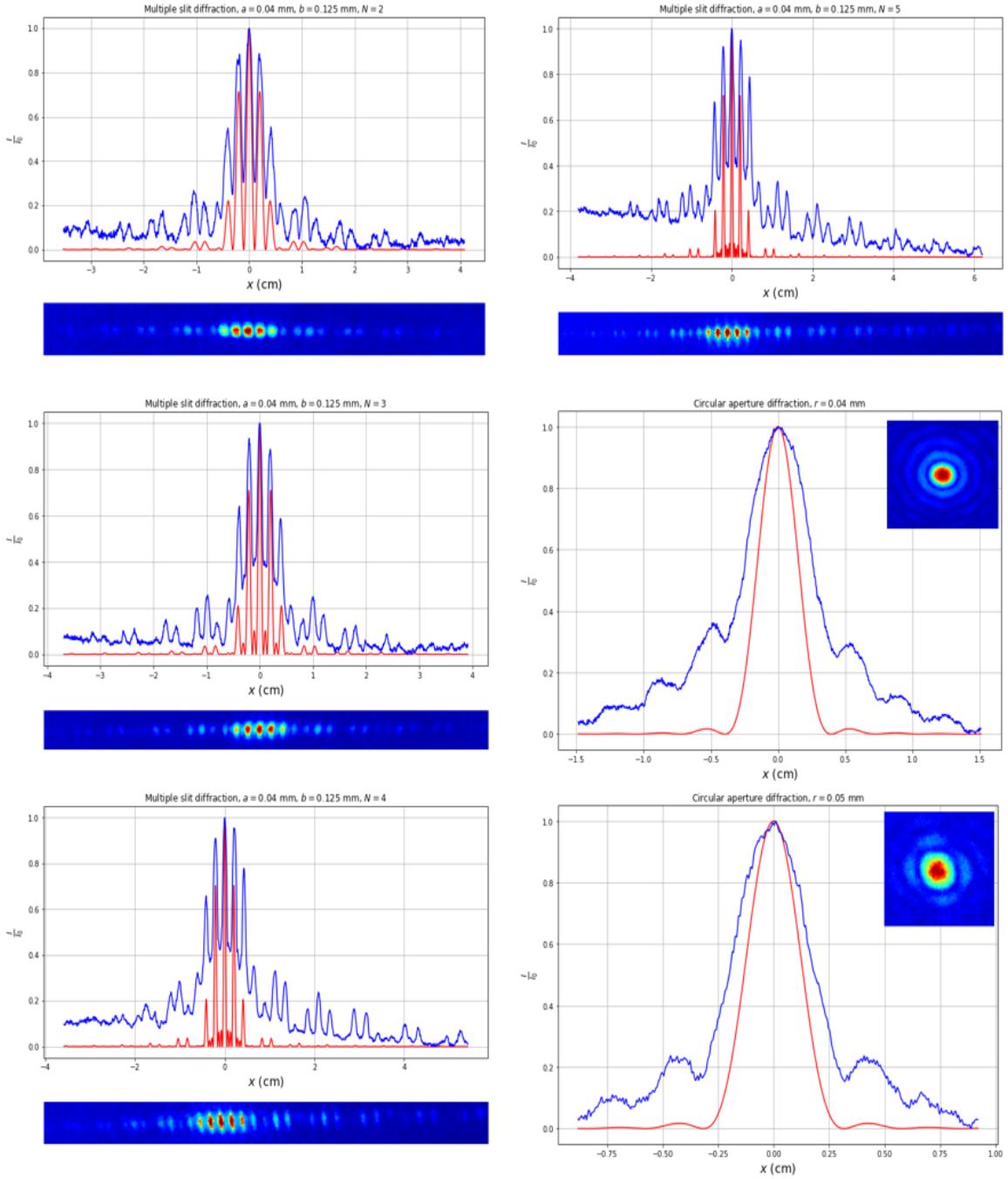

Figure 6: Diffraction patterns for multiple slits and circular apertures. The blue curve is the measured normalized irradiance, and the red curve is the theoretical diffraction curve.

of the central spot exceeded the maximum brightness value that could be measured by the camera, so the relative brightness differences are less pronounced than they should be. Using a camera with a larger brightness capacity or filtering the laser intensity would correct this problem, and make the theoretical and measured diffraction patterns look even more similar.

We also measured the diffraction patterns for opaque points of radii 0.125 and 0.25 mm (Figure 7). The pattern obtained using these obstacles was originally too faint to be seen, so the setup was modified by removing the pinhole and beam expander, and placing a divergent lens a short distance before the screen. We don't attempt to fit for these patterns because the brightness is too large and the intensity distribution too irregular in order to perform a good fit. Qualitatively, however, the patterns conform to expectations, with circular fringes of diminishing brightness surrounding a bright central spot, just like the case of the circular aperture.

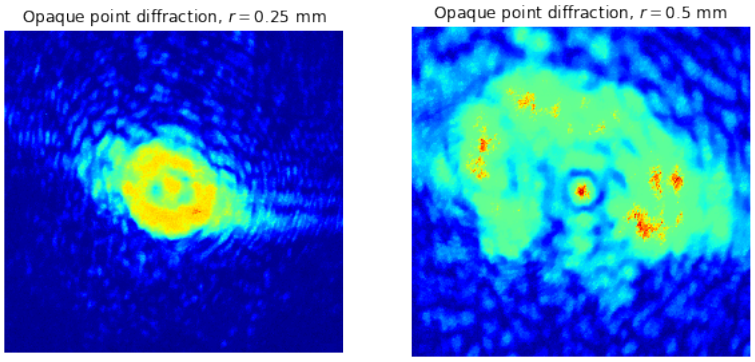

Figure 7: Diffraction patterns for opaque points.

3.2 Experiment 2

3.2.1 Set-Up

This experiment uses the grating formula (3) to find the wavelength of the laser light. The setup is as follows. We set up a target assembly with a diffraction grating on it in front of the laser, and place a large piece of paper as a beam stopper a distance d away from the assembly. We then measure the distances s_1 and s_2 between the zeroth order maximum and the first and second order maxima, respectively. Finally, we turn off the laser and look at the image of a fluorescent lamp through the diffraction grating. All of the distances were measured using a regular ruler.

3.2.2 Results and analysis

For a grating-screen distance of $d = 8.5 \pm 0.1$ cm and a difraction grating of 600 lines/mm, we measured $s_1 = 7.0 \pm 0.1$ cm and $s_2 = 20.7 \pm 0.1$ cm, which corresponds to values of the wavelength of $\lambda_1 = 635 \pm 10$ nm and $\lambda_2 = 644 \pm 3$ nm. The weighted average of the two values gives $\bar{\lambda} = 641 \pm 6$ nm. This corresponds to a discrepancy of $\sim 1.3\%$ with respect to the nominal value of $\lambda = 632.8$ nm.

Small changes in the measured values of s_1 and d can lead to noticeable differences in the calculated wavelength. For instance, using $s_1 = 6.9 \pm 0.1$ cm without varying any of the other values gives $\lambda_1 = 626 \pm 10$ nm, which corresponds to a $\Delta\lambda_1 = 9$ nm. Using $d = 8.3 \pm 0.1$ cm independently gives

$\lambda_1 = 641 \pm 10$ nm and $\lambda_2 = 647 \pm 3$ nm, and thus $\Delta\lambda_1 = \Delta\lambda_2 = 6$ nm. On the other hand, the value of λ_2 is less sensitive to variations in s_2. Using $s_2 = 20.6 \pm 0.1$ cm gives $\lambda_2 = 643 \pm 3$ nm, and thus $\Delta\lambda_2 = 1$ nm. Given these considerations and the relatively low precision of the measuring instrument, it is reasonable that the measured value of the wavelength was not exactly the same as the nominal value.

When we look at the fluorescent lamp through the diffraction grating, we essentially see the light decompose into its respective colors. The formula that describes the irradiance pattern of a multiple slit configuration is sensitive to the wavelength of the incident light, which implies that polychromatic light passing through a diffraction grating will decompose into its constituent wavelengths.

3.3 Experiment 3

3.3.1 Set-Up

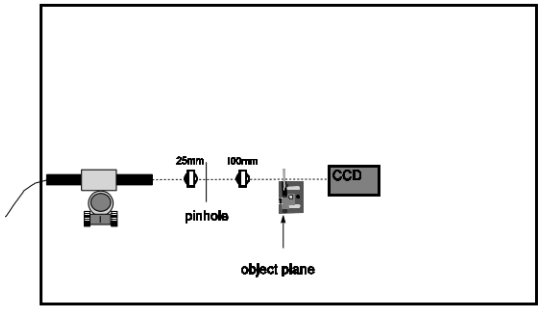

Figure 8: Setup for experiment 3. Obtained from [8].

This experiment attempts to reproduce the Talbot effect. We setup a spatial filter using a 25 mm lens and a pinhole located a distance of 25 mm away from each other, and expand the beam by positioning a 100 mm lens 100 mm away from the pinhole. We then place a target assembly a small distance away from the 100 mm lens and mount a rectangular wire mesh on it such that the incident light passes through it. We then place a CCD camera at a starting distance of 3 cm from the mesh, and take pictures of the pattern captured by the camera at intervals of 10 cm. This setup is illustrated in Figure 8.

3.3.2 Results and analysis

Figures 9 and 10 show the results of the experiment. We used a wire mesh with a period of $a = 0.5$ mm, which gives a Talbot length $z_T \approx 39.5$ cm, and thus we would expect that patterns separated by 40 cm would be very similar to each other. This, however, is not apparent, either in the quantitative SSIM comparison (Figure 10) or by visual inspection (Figure 9). It appears that the patterns in general are simply more similar to their immediate neighbors, but there does not appear to be any surge in the SSIM index at separation distances of 40 cm. The reasons for this are not immediately apparent. The first three images appear to have a different texture than the other six, which is probably due to automatic adjustments made by the camera software, and variations in the distance from the camera to the screen. It is possible that the period of the wire mesh used was not actually 0.5 mm, in which case the Talbot length would be different. A true period of 0.75 mm would imply that $z_T \approx 90$ cm,

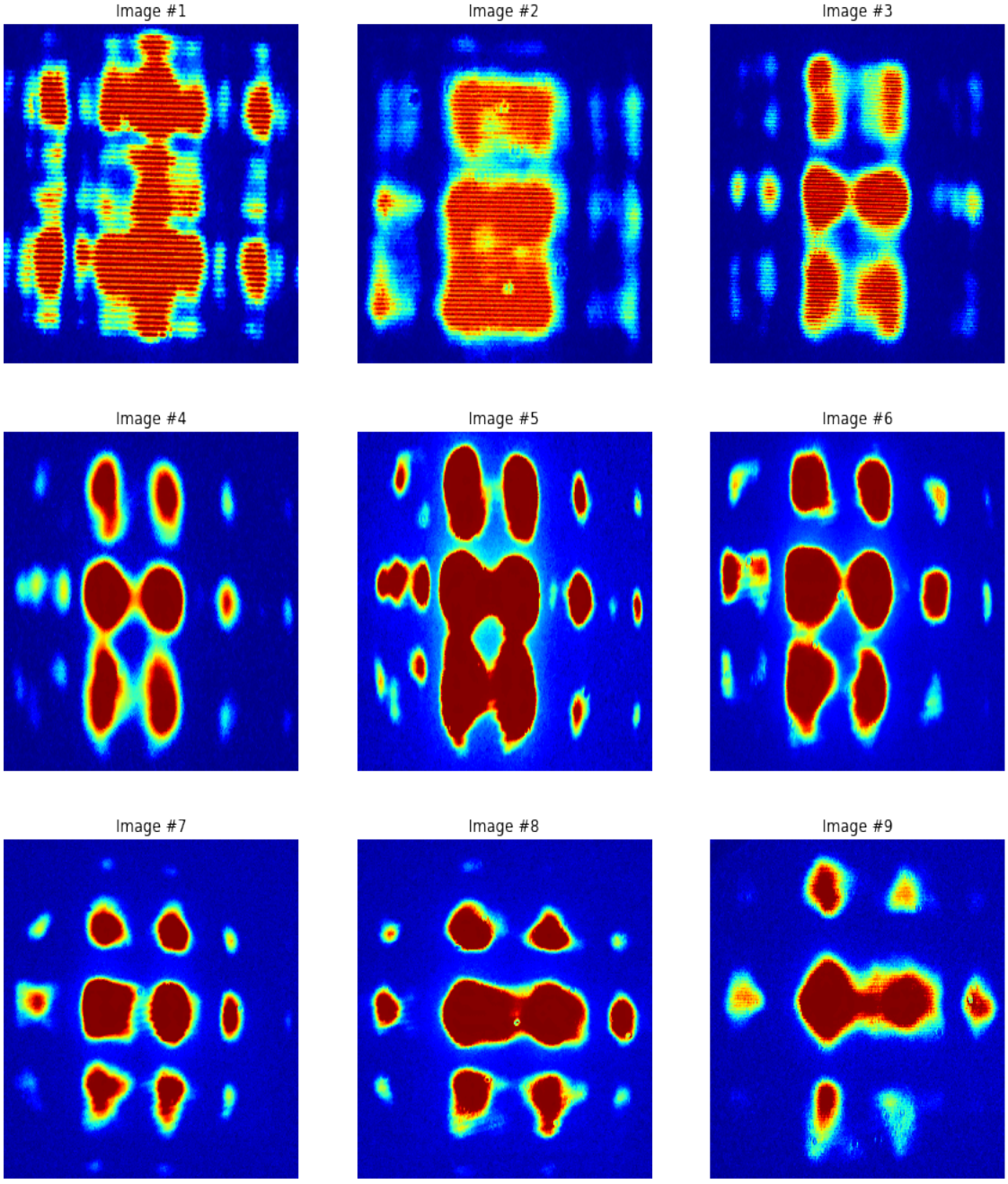

Figure 9: Colormaps of the diffraction patterns obtained for each of the CCD camera's positions. Pictures were taken at 10 cm intervals.

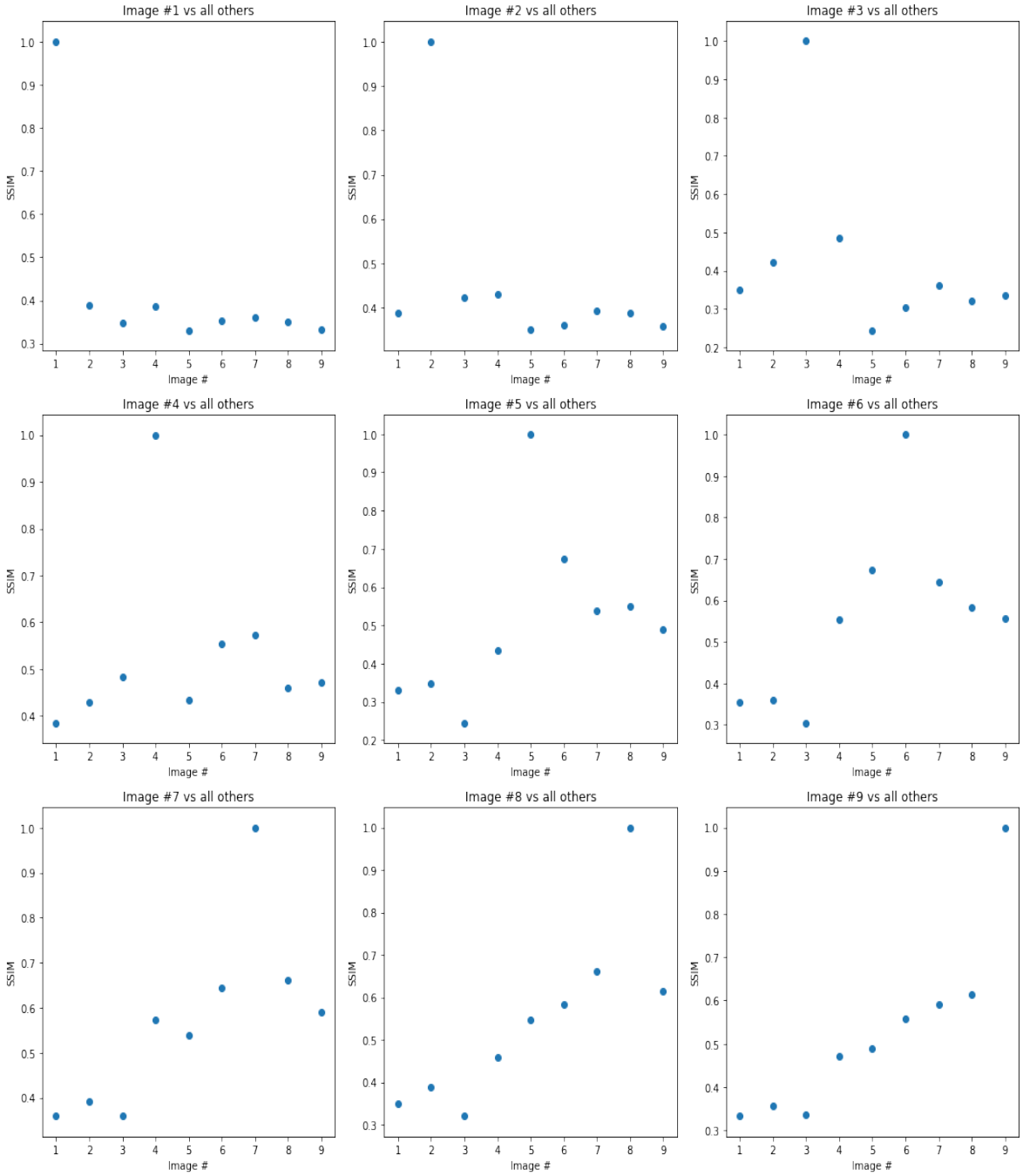

Figure 10: SSIM comparisons between all images.

which would be outside of the sampled range. Periods smaller than 0.3 mm would result in small Talbot lengths that would result in the used sampling rate being less than ideal. Other factors that could have affected the results are the fact that the pictures were cropped manually and artificially resized to matching dimensions. Ideally, this experiment should be repeated using smaller sampling intervals and a larger range, and the diffraction patterns should be transmitted directly from the CCD camera to a computer.

3.4 Experiment 4

3.4.1 Set-Up

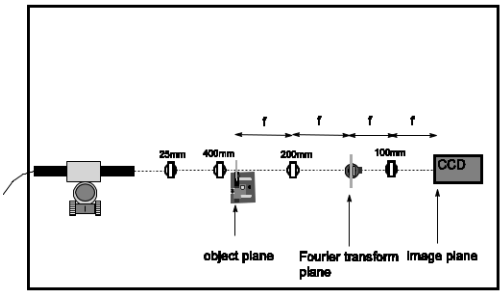

Figure 11: Setup for experiment 4. Obtained from [8].

We now build a coherent optical computer, similar to the one shown in Figure 4. We set up a beam expander using a 25 mm lens and a 400 mm lens at a distance of 425 mm from each other, and position an iris and a target assembly some short distance away from the 400 mm lens, with the iris before the assembly. Then, we set up a second target assembly 400 mm away from the first one, and position a 200 mm lens halfway in between the two. Finally, we set up a CCD camera 200 mm away from the second target assembly, and use a 100 mm lens to bring the light emerging from the second target assembly into focus at the CCD camera by placing it halfway in between the camera and the assembly. Throughout the experiment, we set up different types of apertures at the first target assembly, which constitutes the object plane, and use different types of filters at the second target assembly, whose location corresponds to the Fourier transform plane. The 200 mm lens acts as a Fourier transformer, and the 100 mm lens acts as an inverse Fourier transformer. The setup can is illustrated in Figure 11.

3.4.2 Results and analysis

Figure 12 shows the unfiltered images for each of the apertures used: a rectangular array of circles, a sinusoidal grating, a rectangular wire mesh, and a half-tone image of a duck overlaid with the wire mesh. Figures 13 and 14 shows some of the obtained filtered images for different apertures and filters. We see excellent qualitative agreement between our simulations, obtained by applying equation (8) to the unfiltered images and using the corresponding aperture functions. We can see from the figures that the single slit filter allows us to obtain horizontal lines, that filtering the image using a wire increases the observed frequency of the mesh, and that the single slit filter can also be used to make the mesh disappear. The unfiltered diffraction pattern of the rectangular array of circles is consistent with the array theorem, which states that the diffraction pattern of an array of identical apertures is equal to

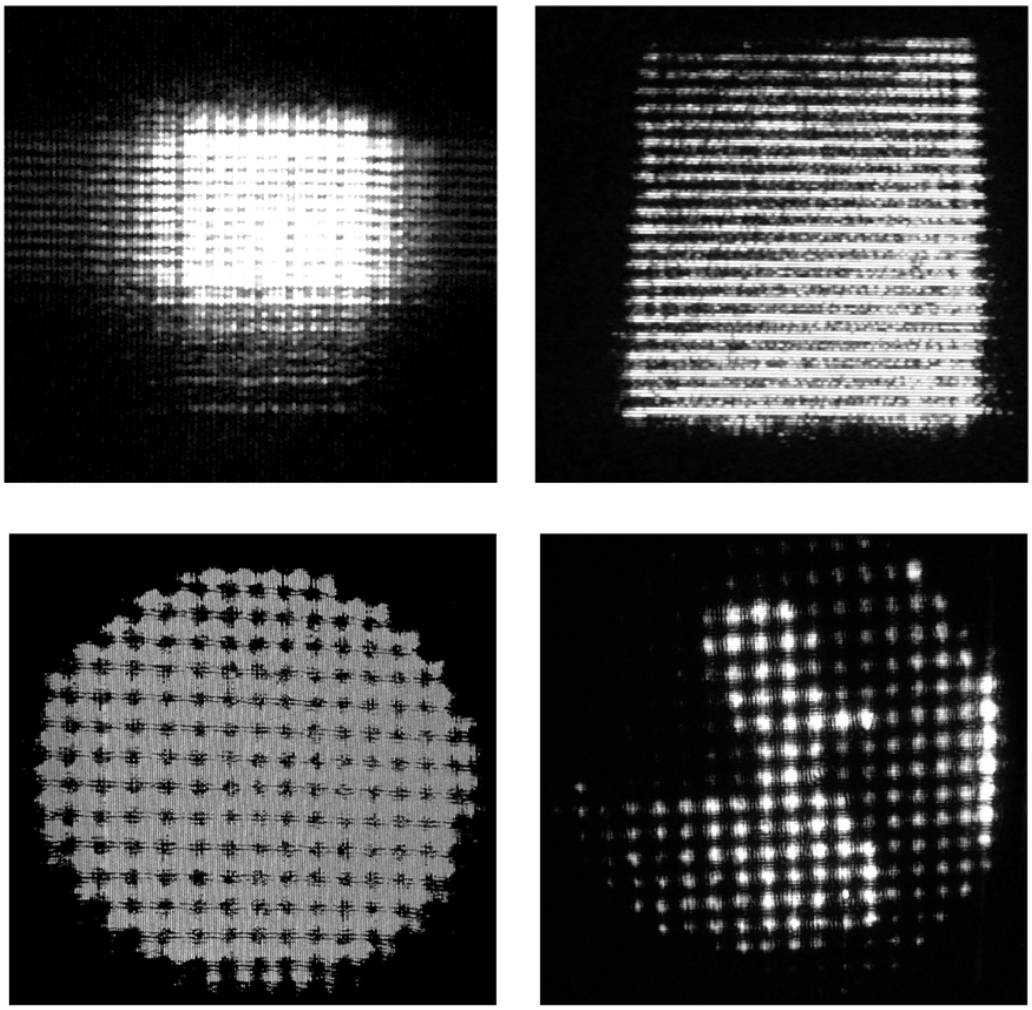

Figure 12: Unfiltered images of the different types of apertures used. Starting from the top left, the types of apertures are: a rectangular array of circles, a sinusoidal grating, a rectangular wire mesh, and a half-tone image of a duck overlaid with the wire mesh.

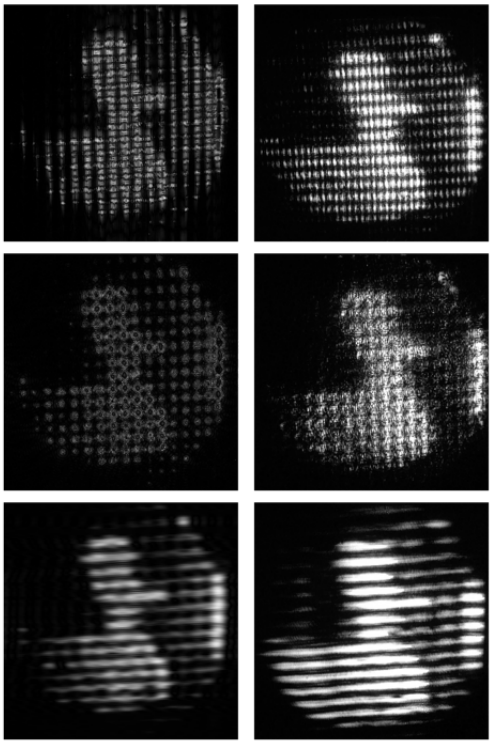

Figure 13: Simulated (left) and observed (right) filtered images of the half-tone duck. From top to bottom, the filters used were a 125 μm wide wire, an opaque dot with 1 mm diameter, and a 0.16 mm single slit.

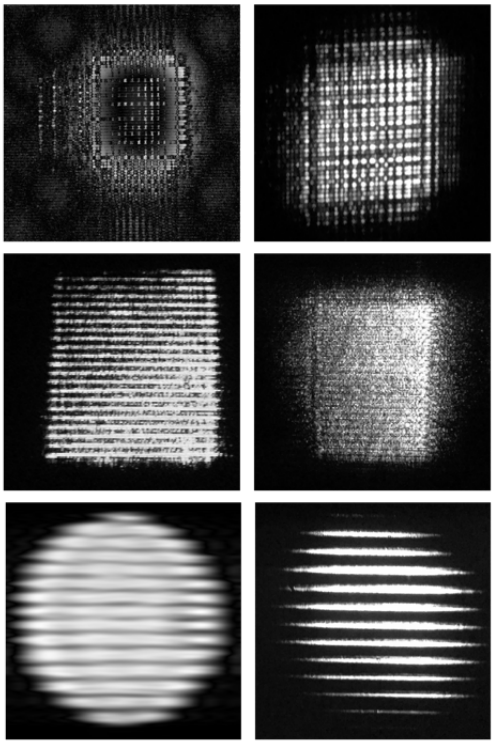

Figure 14: Simulated (left) and observed (right) filtered images. From top to bottom: rectangular array of circles filtered by an opaque dot of diameter 0.5 mm, sinusoidal grating filtered by an opaque dot of diameter 0.25 mm, and wire mesh filtered by a 0.04 mm single slit.

the product of the Fraunhofer diffraction pattern of any of the apertures and the Fourier transform of the locations of each of the apertures.

4 Conclusions

This project's goal was to perform a series of experiments illustrating the phenomenon of diffraction and some of the applications of Fourier optics to solving diffraction problems. Three out of the four experiments performed were successful. We were able to match the theoretical and observed diffraction patterns for different apertures in experiment 1, accurately measure the wavelength of laser light in experiment 3, and numerically reconstruct the filtered diffraction patterns of a coherent optical computer. However, we were unable to successfully observe the Talbot effect. As suggested in section 3.3.2, this failure could be due to a series of different factors, and a careful repetition of the experiment could determine which of these factors constitutes the best explanation. Experiment 1 could be improved by using a camera that has a greater saturation threshold. Better results for experiment 2 could be obtained by using more precise instruments in order to determine distances. For experiment 4, a more sophisticated numerical procedure that took into account more factors like the non zero transparency of the obstacles used as filters, and systematically searched for the optimal aperture function parameters, could potentially yield even better results than those obtained. Directly transferring the images from the CCD camera into a computer would also have been useful.

5 Acknowledgements

The author of this work would like to acknowledge the help received from his lab partner, Juliette Fropier, throughout the data gathering process. I would also like to acknowledge the help provided by our professor, Mukund Vengalattore, and our TA, David Moreau, during lab time.

References

[1] van der Walt, S., et al. *The NumPy Array: A Structure for Efficient Numerical Computation*, Computing in Science & Engineering, 13, 22-30, 2011.

[2] Lebigot, E.O. *Uncertainties: a Python package for calculations with uncertainties*, http://pythonhosted.org/uncertainties/

[3] Hecht, E. *Optics, 5th edit.*, Pearson Education Limited, 2017.

[4] Born, M. & Wolf, E. *Principles of Optics, 7th (expanded) edit.,* Cambridge University Press, 1999.

[5] Berry, M. V., & Klein, S. *Integer, fractional, and fractal Talbot effects.*Journal of Modern Optics, 43, 10, 2139, 1996.

[6] Thomae, D., et al. *Quantitative analysis of imperfect frequency multiplying in fractional Talbot planes and its effect on high-frequency-grating lithography.* J. Opt. Soc. Am. A, 31, 7, 2014.

[7] Wang, Z., et al. *Multiscale structural similarity for image quality assessment.* Conference Record of the Thirty-Seventh Asilomar Conference on Signals, Systems and Computers, 2004. 2: 1398–1402 Vol.2.

[8] Bodenschatz, E., et al. *Modern Experimental Optics Laboratory Manual*, Cornell University Physics Department, 2016.